Atmos. Meas. Tech. Discuss., https://doi.org/10.5194/amt-2019-78
Manuscript under review for journal Atmos. Meas. Tech.
Discussion started: 6 March 2019

Atmospheric Measurement Techniques Discussions

MEMS-based condensation particle counter for real-time monitoring of airborne ultrafine particles at a point of interest

Seong-Jae Yoo[1], Hong-Beom Kwon[1], Ui-Seon Hong[1], Dong-Hyun Kang[2], Sang-Myun Lee[1], Jangseop Han[1], Jungho Hwang[1], Yong-Jun Kim[1]

[1]School of Mechanical Engineering, Yonsei University, Seoul, 03722, Republic of Korea
[2]Micro Nano Fab Center, Korea Institute of Science and Technology, Seoul, 02792, Republic of Korea

Correspondence to: Yong-Jun Kim (yjk@yonsei.ac.kr)

Abstract. We present a microelectromechanical system (MEMS)-based condensation particle counter (CPC) for sensitive and precise monitoring of airborne ultrafine particles (UFPs) at a point of interest that is portable, inexpensive, and accurate. The proposed system consists of two main parts: a MEMS-based condensation chip that grows UFPs to micro-sized droplets and a miniature optical particle counter (OPC) that singly counts grown droplets with the light scattering method. A conventional conductive cooling–type CPC is miniaturized through MEMS technology and the 3D printing technique, and the essential elements for growing droplets are integrated on a single glass slide. The proposed system is much more compact (75 mm × 130 mm × 50 mm), lightweight (205 g), and power-efficient (2.7 W) than commercial CPCs. In quantitative experiments, the results indicated that the proposed system can detect UFPs as small as 13.4 nm by growing them to micro-sized (3.16 μm) droplets. The proposed system measured the UFP number concentration with high accuracy (deviation within 4.1 %), and its detectable concentration range of 7.99–7200 N cm^{-3}. Thus, the proposed system can potentially be used for UFP monitoring in both low-concentration (e.g., air filtration system, high-precision industries utilizing cleanrooms) and high-concentration (e.g., indoor/outdoor atmospheres) environments.

1 Introductions

Monitoring of airborne ultrafine particles (UFPs), which are smaller than 100 nm, is needed in various fields for human health and yield enhancement in industrial fields(Donaldson et al., 1998; Donovan et al., 1985; Hristozov and Malsch, 2009). UFPs are mainly generated from burning fossil fuels and are ubiquitous in urban air; they account for about 90% of the total particle number concentration(Kittelson, 1998; Shi et al., 1999). Because of dramatic developments in nanotechnology, engineered UFPs for commercial and research purposes have been produced at a large scale. These incidentally and intentionally generated UFPs are more harmful to human health than larger counterparts: UFPs have a higher chance to deposit in the lower respiratory system and are more toxic owing to their larger surface-to-volume ratios, which causes oxidative stress, pulmonary inflammation, and tumor development(Hext, 1994; Li et al., 2003; Renwick et al., 2004). Thus, onsite monitoring is needed to assess and minimize UFP exposure. High-precision industries with cleanrooms also need UFP monitoring to increase the production yield. For instance, in the semiconductor industry, the minimum linewidth of the chips is approaching 7 nm(Neisser and Wurm, 2015). Particles that are a few nanometers in size are critical because “killer particles” (i.e., the diameter is greater than half of the minimum linewidth) can render the whole chip unusable(Libman et al., 2015). Unfortunately, since UFPs in cleanrooms are generated during fabrication processes (e.g., chemical vapor deposition (CVD), metallization, wet etching), contamination can occur in any manufacturing stages(Choi et al., 2015; Manodori and Benedetti, 2009). In these circumstances, a portable and low-cost sensor is needed for onsite UFP monitoring to accurately evaluate adverse health effects and control the contamination level in cleanrooms to enhance the production yield.

Condensation particle counters (CPCs) are one of the most widely used UFP detection instruments and are based on the heterogeneous particle condensation technique(Stolzenburg and McMurry, 1991). They grow UFPs to micro-sized droplets through condensation and count them by optical means. Compared to other detection techniques (e.g., electrical and

gravitational methods), CPCs provide extremely sensitive and precise counting because they are theoretically capable of counting every single UFP(Kangasluoma et al., 2017; Kangasluoma et al., 2014; McMurry, 2000). Moreover, if a differential mobility analyzer (DMA) is used as a particle size selector, CPCs can offer higher particle size resolution (64 size channels per decade) than any other particle-sizing instruments(Sioutas, 1999; Stolzenburg et al., 2017). However, commercially available CPCs are bulky and expensive; thus, they are impractical for onsite monitoring where the UFP concentration changes continuously. Although portable CPCs (model 3007, TSI Inc., USA) are currently on the market, they are still large in size (292 mm × 140 mm × 140 mm) and expensive (~10,000 USD) for ownership. Therefore, despite their advantages, CPCs are difficult to actively utilize for onsite monitoring applications.

In the past few years, several studies have used microelectromechanical system (MEMS) technology for UFP analysis(Hajjam et al., 2010; Kang et al., 2012; Kim et al., 2018; Kim et al., 2015; Wasisto et al., 2013; Zhang et al., 2016). Because this technology is capable of batch- and micro-size fabrications through the semiconductor manufacturing process, such chips provide cost-efficiency, compactness, and enhanced portability. Most MEMS-based sensors developed for monitoring UFPs were based on the electrical technique. However, these sensors exhibited low sensitivity because their small size means that they have to operate at a small volumetric flow rate (below 1 LPM), and UFPs carry small charges because of their limited surface area.

In this study, we developed a high-performance MEMS-based CPC that is portable, inexpensive, and power-efficient. The proposed system comprises a MEMS-based condensation chip and miniature optical particle counter (OPC). UFPs are grown to micrometer-sized droplets on the chip, and the grown droplets are detected by the miniature OPC. Owing to the MEMS and 3D printing technologies, particle enlargement (i.e., the fundamental process of the CPC) can be realized on a chip-scale system because the essential elements for growing droplets (i.e., channels, micropillar-type wick, heaters, temperature sensors) are integrated on a single glass slide. Accordingly, the proposed system has a size of 75 mm × 130 mm × 50 mm, weight of 205 g, and power consumption of 2.7 W. Moreover, the MEMS-based condensation chip is a cartridge type; it can easily be exchanged after a long operation time and simply connected to the control circuit board.

In addition to its compactness, the proposed system also provides high degrees of accuracy and precision. A quantitative characterization using Ag particles indicates that the proposed system can detect individual particles with a size of 13.6 nm and measure the UFP number concentration within a difference of 9.13 % compared to commercial CPCs. These results show that our system can potentially be used as a portable, low-cost, and high-precision UFP sensor for various fields (e.g., assessing UFP exposure, monitoring workplaces, tracing particle sources in high-precision industries with cleanrooms). Moreover, when combined with the recently developed miniature DMA, the proposed system should also be able to perform onsite monitoring of the UFP size distribution with high resolution(Liu and Chen, 2016; Qi and Kulkarni, 2016).

2 Description of the MEMS-based CPC

Figure 1 shows the operating principle of the proposed MEMS-based CPC, which consists of a reservoir, saturator, condenser, and miniature OPC. To generate supersaturated vapor and hence grow UFPs to micro-sized droplets, the proposed system utilizes a conductive cooling method. The saturator generates saturated vapor by heating the wetted wall with the working fluid. This saturates the UFP-laden sample, which is introduced into the saturator at a flow rate of 0.15 LPM, with working fluid vapor. The saturated sample then enters a condenser, whose temperature (10 °C) is lower than that of the saturator (40 °C). In the condenser, the hot saturated vapor present in the sample is cooled to reach the supersaturated state. UFPs in the supersaturated vapor act as condensational nuclei and grow to droplets. The mean diameter of grown droplets are 3.16 μm, which can be easily detected by the miniature OPC based on the light scattering method. The experimental results of the droplet size distribution are included in the supplemental material (Figure S1).

Atmos. Meas. Tech. Discuss., https://doi.org/10.5194/amt-2019-78
Manuscript under review for journal Atmos. Meas. Tech.
Discussion started: 6 March 2019

The cornerstone of the proposed system is its compact, cost-efficient, and portable features for the onsite monitoring of UFPs. Figure 2a shows an optical image of the proposed system. By using the MEMS technology, the proposed system can generate supersaturated vapor and grow droplets on a chip-scale system for significant decreases in the size, weight, and power consumption. The heaters, temperature sensors, and wick are monolithically integrated with the glass slide (Figure 2b) and perform crucial roles: supplying the working fluid to the saturator and condenser via capillary action and generating supersaturated vapor.

As shown in Figure 2c, micropillar arrays serve as a wick with dimensions of 40 μm in diameter, 100 μm in length, and 100 μm in pitch. A micropillar-type wick with these dimensions was experimentally determined to be capable of pumping the working fluid from the reservoir and spreading it over the entire surface of the saturator to ensure that the saturator wall is always in the wetted condition. SU-8 is a negative-tone photoresist and was chosen as the structural material of the micropillar-type wick because it provides a high patterning resolution (~ 1 μm) and outstanding chemical/thermal stability to guarantee the high durability of the proposed system(Chang and Kim, 2000; Kim et al., 2003).

In order to generate supersaturated vapor with a constant saturation ratio, the temperatures of the saturator (40 °C) and condenser (10 °C) must be controlled to the designed values. For this purpose, the resistive heater was uniformly patterned on the inner wall of the saturator, and a miniature thermoelectric cooling module was attached to the outer wall of the condenser. Both temperatures were monitored with resistive temperature sensors having an accuracy of ± 0.1 °C and located at the outlet of the saturator and center of the condenser, respectively. A customized circuit was used with the pulse width modulation (PWM) method to adjust the power for the heaters and thermoelectric cooler module and thus control the temperatures.

In the condenser, while supersaturated vapor grows UFPs to droplets, some may condense on the wall and clog the channel. Thus, like the saturator, the condenser also had micropillar-type wicks to prevent droplet formation on the wall and drain the condensed working fluid to the reservoir. While the diameter and length were the same, the pitch of the micropillar-type wick was larger than that in the saturator. This is because permeability is preferred over the capillary force for a rapid discharge of the working fluid.

A spacer, which included the channels and inlet/outlet connectors, was fabricated with a 3D printer in a single printout. The material for the spacer was UV-curable epoxy, which has a high printing resolution (minimum linewidth: 0.3 mm) and can endure temperatures up to 80 °C(Stansbury and Idacavage, 2016). The channel of the saturator was winding to increase the residence time and thus ensure fully saturated vapor. The width, height, and length of the saturator channel were 6, 3, and 150 mm, respectively, and the corresponding residence time at the given flow rate was 1.08 s. The maximum Reynolds number in the channel at the given flow rate was only 32, which means that the sample stream in the channel was in the fully laminar regime.

3 Fabrication process

As shown in Figure 3, the MEMS-based particle growth system consists of a top plate, bottom plate, and 3D-printed channel. The fabrication process was identical for the two plates. The essential elements on the plates (heaters, resistive temperature sensors, and micropillar-type wick) were fabricated through a simple photolithographic process. An E-beam evaporator was used to deposit a thin metal layer (30/300 nm of Ti/Au) on the plates. Then, a positive-tone photoresist was spin-coated at 3000 rpm for 30 s, and softly baked on a hot plate at 95 ℃ for 1 min. After baking, the photoresist was exposed to UV light (wavelength: 365 nm, exposure dose: 55 mJ cm^{-2}) and developed with a photoresist developer. Then, the wet etching process was performed to define the electrodes (Figure 3a). To enhance the repeatability of the temperature sensors, the fabricated electrodes were heat-treated at 300 °C in ambient atmosphere. The SU-8 negative-tone photoresist was used as the material for the micropillar arrays. A 100 μm layer of SU-8 (model 2100, Microchem Corp., USA) was spin-coated onto the plates at 3000 rpm for 30 s and baked at 85 °C for 120 min. Then, it was exposed to UV light (exposure dose: 240 mJ cm^{-2}) to define

the micropillar array structure. Next, a post-exposure-bake (PEB) was conducted through a two-step ramping process on a hot plate: 65 °C for 5 min and then 95 °C for 120 min. The exposed SU-8 was developed with a SU-8 developer (Figure 3b).

The fabricated channel and plates were packaged with polymethyl methacrylate (PMMA) jigs and silicon rubber gaskets (Figure 3c). The cooling modules comprised a thermoelectric cooler, heat sink, and mini fan and were attached to the outer walls of the condenser (Figure 3d). Finally, the fabricated chip was inserted into a card connector, which was linked to the control circuit board.

4 Experimental setup

Figure 4 shows the experimental setup used to characterize the overall performance of the proposed system in terms of three aspects: (a) the clean air supply system, (b) monodisperse particle generating system, and (c) performance comparison system. Compressed air was used as the carrier gas. Any moisture, oil droplets, and particles in the compressed air were removed in the clean air supply system with an oil trap, diffusion dryer, and high-efficiency particulate (HEPA) filter. The purified air was then supplied to the particle generating system at a flow rate that was accurately controlled by a mass flow controller (MFC; VIC-D200, MKP Co., KR). Ag particles ranging in size from 4 nm to 40 nm were generated by an Ag particle generator (EP-NGS20, EcoPictures Co., KR). They were electrically charged by a soft X-ray charger (XRC-05, HCT Co., KR) and then classified to a specific diameter with a DMA (model 3081A, TSI Co. Ltd., USA). Next, the number concentration of the monodisperse Ag particles were controlled (0–7200 N cm^{-3}) in the dilution bridge system by adjustment of the needle valve. Finally, the concentration-controlled and monodisperse Ag particles were introduced into the proposed system and reference instrument, which was either a CPC (model 3772, TSI Inc., USA) or aerosol electrometer (model 3068B, TSI Inc., USA). The lengths of tubes that led to the proposed system and reference instrument were carefully adjusted to guarantee the same transport times.

5 Results and discussion

5.1 Working fluid transmission and evaporation

In order to characterize the wick capability of the working fluid transmission and evaporation, a rectangular test sample was used. The sample included a heater and temperature sensor, and its length was equal to the saturator maximum length (38 mm) of the proposed system.

To identify the supply capability of the wick, a capillary rise experiment was performed (Figure 5a). The sample was slowly lowered to the surface of the working fluid. Once the bottom of the sample touched the surface (t = 0 s), the rise of the working fluid on the sample was recorded. As shown in Figure 5b, the forefront of the working fluid rose rapidly at the beginning and then slowed down gradually. The forefront of the working fluid reached the endpoint of the saturator in 35 s and thus wetted the whole surface of the sample.

In the saturator, the working fluid transported by the wick is vaporized at elevated temperatures. When the rate of the working fluid evaporation is higher than that of the transportation, a dry-out region is formed. This phenomenon must be minimized because the partial vapor pressure near the wall must be kept close to the saturated condition. Figure 5c shows optical images of the dry-out region formation as the surface temperature increased. The temperature of the sample surface was increased in increments of 10 °C; at each temperature, the system operated for 180 s. The dry-out region clearly did not form when the surface temperature was equal to the designed saturator temperature (40 °C) and even reached 70 °C. At 80 °C, the front of the working fluid started to recede, so a dry out-region formed. At 90 °C, the area of the dry-out region accounted for approximately 20 % of the heated surface. These results demonstrate that the amount of the working fluid supplied from the wick was greater than the rate of evaporation in the condenser at the design temperature. Moreover, the saturator temperature

Atmos. Meas. Tech. Discuss., https://doi.org/10.5194/amt-2019-78
Manuscript under review for journal Atmos. Meas. Tech.
Discussion started: 6 March 2019

can be raised to 70 °C to increase the saturation ratio and hence decrease the Kelvin diameter to enabling the system to detect smaller particles.

5.2 Size-dependent particle counting efficiency

The counting efficiency (η_d) is defined as the efficiency of the system at detecting the drawn particles and describes the overall CPC performance. It is the product of three efficiencies:

$$\eta_d = \eta_{trans} \cdot \eta_{act} \cdot \eta_{OPC}, \quad (1)$$

where η_{trans}, η_{act}, and η_{OPC} are the efficiencies of a particle passing through the proposed system, the condensation chip at growing droplets, and the OPC at counting droplets passing through its sensing volume, respectively. Because these three efficiencies are strongly dependent on the particle size, the counting efficiency must be characterized as a function of the particle size.

The counting efficiency was obtained from the ratio of the concentration measured with the proposed system to the reference number concentration. The reference concentration (N_{ref}) was obtained from the electrical current (I) measured by the AE:

$$I = N_{ref} \cdot ne \cdot Q, \quad (2)$$

where n is the number of elementary charges (+1) per particle, e is the elementary charge (1.6×10^{-19} C), and Q is the flow rate drawn into the AE.

Figure 6 shows the size-dependent counting efficiency of the MEMS-based CPC. The number concentration range of Ag particles was controlled to be 1000–2000 N cm^{-3}. Our system initially detected nanoparticles at 5 nm, and the detection efficiency increased sharply above 9 nm. This was primarily because the activation efficiency (η_{act}) increased when the particle size exceeded the Kelvin diameter (2.45 nm). The transport efficiency (η_{trans}) increased as the diffusion loss decreased because the diffusivity of a particle is inversely proportional to its size. The corresponding minimum detectable size is defined as the size at which particles are detected with 50% efficiency and was found to be 13.4 nm. The detection efficiency was 90% at 20.6 nm and reached 95% at 22.9 nm; this indicates that particle losses by various particle deposition mechanisms (e.g., thermophoresis, diffusion, impaction) were negligible.

5.3 Detectable concentration range

Even if filtered air is introduced into a system, droplets may form in the condenser via homogeneous or ion-induced nucleation. Droplets without UFP nuclei cause false counting, which makes the system read a higher concentration than reality. This phenomenon is critical, especially in low-concentration environments. To evaluate the false counting of the proposed system, it was operated for 1 h with a HEPA filter connected to its inlet. When the temperature difference between the saturator and condenser was set to 30 °C, the average number concentration during the measurement period (background concentration) was only 0.05 N cm^{-3}. This result indicated that homogeneous nucleation hardly occurred. Thus, the temperature profile was uniformly established inside the condensation chip because homogeneous nucleation typically occurs at low temperatures in regions where the local saturation ratio is high.

We characterized the maximum detectable number concentration of our system by comparing the number concentration with that of the aerosol electrometer (i.e., reference number concentration). Monodisperse Ag particles with a size of 25 nm were used as the test particle, and their number concentration was increased in intervals of 3 min. Figure 7 shows (a) the time series of number concentrations measured with the MEMS-based CPC and an aerosol electrometer and (b) a one-to-one comparison of the measured number concentrations by both systems. As shown in Figure 7b, relatively large fluctuations were observed at number concentrations of < 1000 N cm^{-3} because the lower concentration limit of the aerosol electrometer was relatively high (1 fA = 375 N cm^{-3} at 1 LPM). However, at the number concentration range of 1000–5000 N cm^{-3}, the overall difference between the concentrations of our system and the aerosol electrometer was only 4.1 %, which proves the high accuracy of our system. When the concentrations exceeded 5000 N cm^{-3}, the deviation between the measured and reference number

concentrations gradually increased. One of the main reason was the coincidence error. When multiple particles simultaneously passed through the sensing volume, the miniature OPC could not count them separately. The maximum detectable concentration of our system, which was defined as the number concentration at a difference of 20 %, was 7200 N cm^{-3}. The maximum detectable concentration can be increased by adopting a photometric method utilized by commercial CPCs: if the environmental concentration is above the maximum detectable concentration, the system measures the time-averaged value of analog signals from the photodetector and converts it to the number concentration based on previously obtained empirical data.

5.4 Performance comparison with the reference CPC

The MEMS-based CPC was tested in parallel with a reference CPC. The classification voltage of the DMA was changed to introduce monodisperse Ag particles varying in concentration and size into both systems. The total measurement time was 600 s, and the measured data were averaged in intervals of 6 s. Figure 8 shows the measured number concentrations of the proposed system and reference CPC. When particles larger than the minimum detectable size (13.4 nm) were introduced, the proposed system clearly showed high accuracy and precision comparable to those of the reference CPC: a difference of 4.54 % difference at a low concentration (7.99 N cm^{-3} at 28 nm) and -9.13 % difference at a high concentration (4544.82 N cm^{-3} at 16 nm).

6 Conclusion

The MEMS-based CPC was developed for sensitive and precise monitoring of UFPs at a particular point of interest. Our system comprises two parts: the MEMS-based condensation chip and miniature OPC. To achieve compactness, the key elements for growing droplets (i.e., a saturator, reservoir, and condenser) were integrated on a 52.5 mm × 60 mm glass slide through a simple photolithographic process and 3D printing. Quantitative experiments with an aerosol electrometer (AE; model 3068B, TSI Inc., USA) and CPC (model 3772, TSI Inc., USA) demonstrated that our system can count UFPs with a size of 13.4 nm and measure the number concentration with high accuracy (within 4.1 % difference compared to AE) in the range of 1000–5000 N/cm^3.

In terms of compactness and cost-efficiency, the proposed system is superior to conventional instruments. The proposed system has a far smaller physical volume than the reference CPCs and is less than 91.5 % of the portable CPC (model 3007, TSI Inc., USA) available in the market. Furthermore, its manufacturing cost can be minimized owing to batch fabrication based on MEMS technology. These advantages allow the system to be successfully applied to various fields that require UFP monitoring. Furthermore, if combined with the recently developed miniature DMA, our system can help realize a mini-scanning mobility particle sizer (mini-SMPS) for accurate and precise measurement of the UFP size distribution at particular point of interest.

Author contributions

S.J.Y., H.B.K., and Y.J.K. conceptualized the study. H.B.K., U.S.H., S.J.Y., D.H.K., and S.M.L. performed the experimental work. S.J.Y. wrote the original draft, and S.J.Y., H.B.K., and D.H.K revised it. J.H. and J.H. provided the resources. All authors discussed and commented on the manuscript and approve of its content.

Competing interests

The authors declare that they have no conflict of interest.

Acknowledgements

This work was supported by Samsung Research Funding & Incubation Center of Samsung Electronics under Project Number SRFC-TA1803-05 and by the Technology Innovation Program (10077651, Development of IoT fusion sensor system based on artifcial intelligence) funded by the Ministry of Trade, Industry & Energy (MOTIE, Korea).

References

Chang, H.-K. and Kim, Y.-K.: UV-LIGA process for high aspect ratio structure using stress barrier and C-shaped etch hole, Sensors and Actuators A: Physical, 84, 342-350, 2000.

Choi, K.-M., Kim, J.-H., Park, J.-H., Kim, K.-S., and Bae, G.-N.: Exposure characteristics of nanoparticles as process by-products for the semiconductor manufacturing industry, Journal of occupational and environmental hygiene, 12, D153-D160, 2015.

Donaldson, K., Li, X., and MacNee, W.: Ultrafine (nanometre) particle mediated lung injury, Journal of Aerosol Science, 29, 553-560, 1998.

Donovan, R., Locke, B., Osburn, C., and Caviness, A.: Ultrafine aerosol particles in semiconductor cleanrooms, Journal of The Electrochemical Society, 132, 2730-2738, 1985.

Hajjam, A., Wilson, J. C., Rahafrooz, A., and Pourkamali, S.: Fabrication and characterization of resonant aerosol particle mass sensors, 2010, 863-866.

Hext, P.: Current perspectives on particulate induced pulmonary tumours, Human & experimental toxicology, 13, 700-715, 1994.

Hristozov, D. and Malsch, I.: Hazards and risks of engineered nanoparticles for the environment and human health, Sustainability, 1, 1161-1194, 2009.

Kang, J. S., Lee, K. S., Lee, K. H., Sung, H. J., and Kim, S. S.: Characterization of a microscale cascade impactor, Aerosol Science and Technology, 46, 966-972, 2012.

Kangasluoma, J., Hering, S., Picard, D., Lewis, G., Enroth, J., Korhonen, F., Kulmala, M., Sellegri, K., Attoui, M., and Petäjä, T.: Characterization of three new condensation particle counters for sub-3 nm particle detection during the Helsinki CPC workshop, Atmospheric Measurement Techniques, 2017. 2017.

Kangasluoma, J., Kuang, C., Wimmer, D., Rissanen, M., Lehtipalo, K., Ehn, M., Worsnop, D., Wang, J., Kulmala, M., and Petäjä, T.: Sub-3 nm particle size and composition dependent response of a nano-CPC battery, Atmospheric Measurement Techniques, 7, 689-700, 2014.

Kim, H.-L., Han, J., Lee, S.-M., Kwon, H.-B., Hwang, J., and Kim, Y.-J.: MEMS-based particle detection system for measuring airborne ultrafine particles, Sensors and Actuators A: Physical, 283, 235-244, 2018.

Kim, H.-L., Han, J. S., Lee, S.-M., Kwon, H.-B., Hwang, J., and Kim, Y.-J.: Ultrafine particle counter using a MEMS-based particle processing chip, 2015, 559-562.

Kim, J.-S., Kang, J.-W., and Kim, J.-J.: Simple and low cost fabrication of thermally stable polymeric multimode waveguides using a UV-curable epoxy, Japanese journal of applied physics, 42, 1277, 2003.

Kittelson, D. B.: Engines and nanoparticles: a review, Journal of aerosol science, 29, 575-588, 1998.

Li, N., Sioutas, C., Cho, A., Schmitz, D., Misra, C., Sempf, J., Wang, M., Oberley, T., Froines, J., and Nel, A.: Ultrafine particulate pollutants induce oxidative stress and mitochondrial damage, Environmental health perspectives, 111, 455-460, 2003.

Libman, S., Wilcox, D., and Zerfas, B.: Ultrapure Water for Advance Semiconductor Manufacturing: Challenges and Opportunities, ECS Transactions, 69, 17-28, 2015.

Liu, Q. and Chen, D.-R.: Experimental evaluation of miniature plate DMAs (mini-plate DMAs) for future ultrafine particle (UFP) sensor network, Aerosol Science and Technology, 50, 297-307, 2016.

Manodori, L. and Benedetti, A.: Nanoparticles monitoring in workplaces devoted to nanotechnologies, 2009, 012001.

McMurry, P. H.: The history of condensation nucleus counters, Aerosol Science & Technology, 33, 297-322, 2000.

Neisser, M. and Wurm, S.: ITRS lithography roadmap: 2015 challenges, Advanced Optical Technologies, 4, 235-240, 2015.

Qi, C. and Kulkarni, P.: Miniature differential mobility analyzer for compact field-portable spectrometers, Aerosol Science and Technology, 50, 1145-1154, 2016.

Renwick, L., Brown, D., Clouter, A., and Donaldson, K.: Increased inflammation and altered macrophage chemotactic responses caused by two ultrafine particle types, Occupational and Environmental Medicine, 61, 442-447, 2004.

Shi, J. P., Khan, A., and Harrison, R. M.: Measurements of ultrafine particle concentration and size distribution in the urban atmosphere, Science of the Total Environment, 235, 51-64, 1999.

Sioutas, C.: Evaluation of the measurement performance of the scanning mobility particle sizer and aerodynamic particle sizer, Aerosol Science & Technology, 30, 84-92, 1999.

Stansbury, J. W. and Idacavage, M. J.: 3D printing with polymers: Challenges among expanding options and opportunities, Dental Materials, 32, 54-64, 2016.

Stolzenburg, D., Steiner, G., and Winkler, P. M.: A DMA-train for precision measurement of sub-10 nm aerosol dynamics, Atmospheric Measurement Techniques, 10, 1639-1651, 2017.

Stolzenburg, M. R. and McMurry, P. H.: An ultrafine aerosol condensation nucleus counter, Aerosol Science and Technology, 14, 48-65, 1991.

Wasisto, H. S., Merzsch, S., Waag, A., Uhde, E., Salthammer, T., and Peiner, E.: Airborne engineered nanoparticle mass sensor based on a silicon resonant cantilever, Sensors and Actuators B: Chemical, 180, 77-89, 2013.

Zhang, C., Zhu, R., and Yang, W.: A micro aerosol sensor for the measurement of airborne ultrafine particles, Sensors, 16, 399, 2016.

Atmos. Meas. Tech. Discuss., https://doi.org/10.5194/amt-2019-78
Manuscript under review for journal Atmos. Meas. Tech.
Discussion started: 6 March 2019

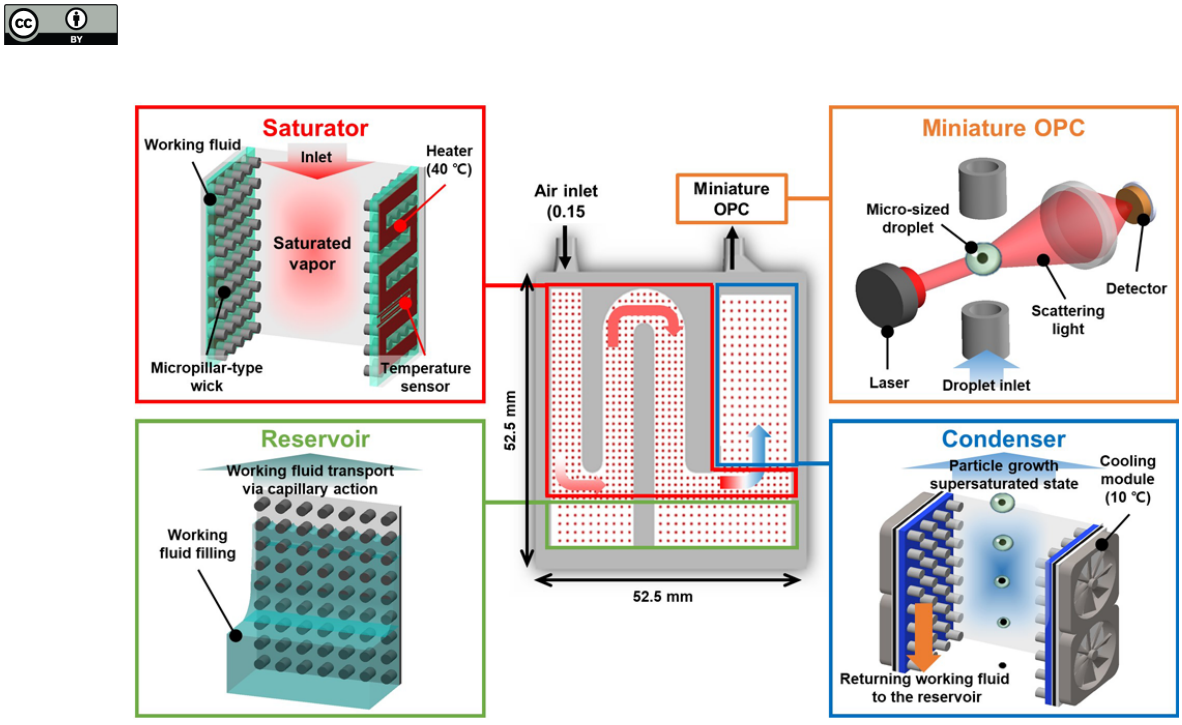

Figure 1: Schematic illustration of the MEMS-based CPC. The proposed system consists of four parts: the reservoir, saturator, condenser, and miniature OPC. The reservoir supplies the working fluid to the saturator via capillary action by the micropillar-type wick. The saturator heats the working fluid to generate saturated vapor. The saturated air becomes supersaturated when cooled by the condenser. UFPs grow into micro-sized droplets in the condenser and are counted by the miniature OPC.

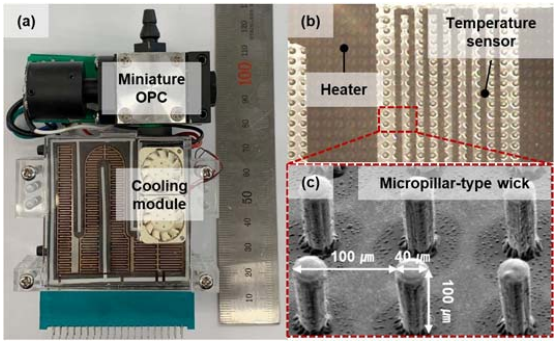

Figure 2: (a) Optical image of the proposed system; (b) magnified image of the heaters, resistive temperature sensors, and wick on the glass slide; and (c) scanning electron microscope (SEM) image of the micropillar-type wick.

Atmos. Meas. Tech. Discuss., https://doi.org/10.5194/amt-2019-78
Manuscript under review for journal Atmos. Meas. Tech.
Discussion started: 6 March 2019

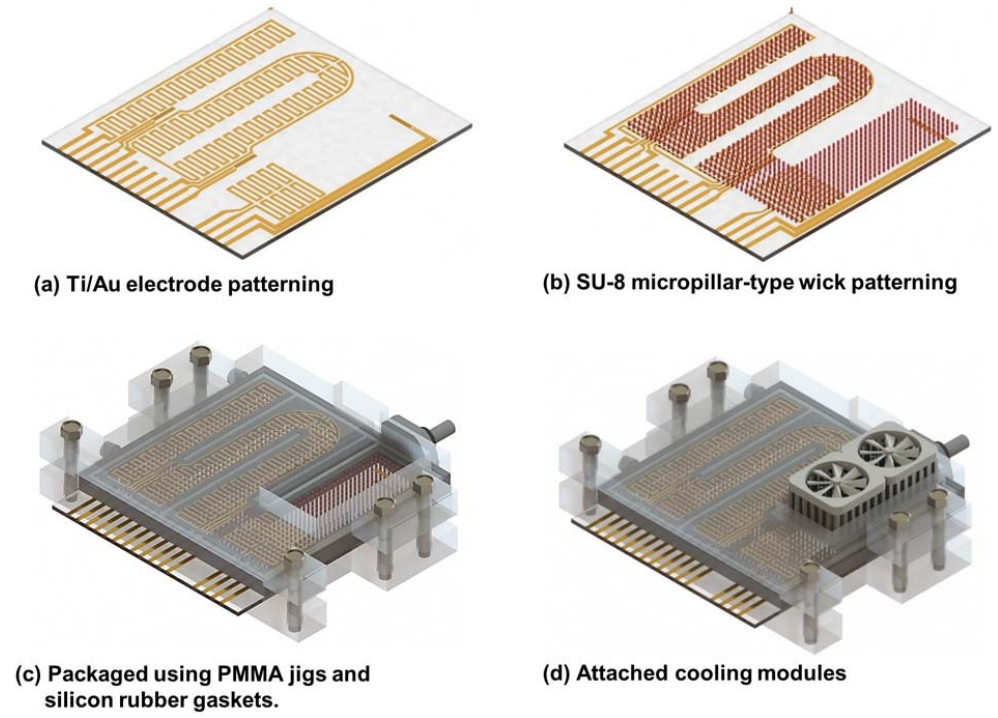

Figure 3: Simplified fabrication process of the MEMS-based CPC.

Atmos. Meas. Tech. Discuss., https://doi.org/10.5194/amt-2019-78
Manuscript under review for journal Atmos. Meas. Tech.
Discussion started: 6 March 2019

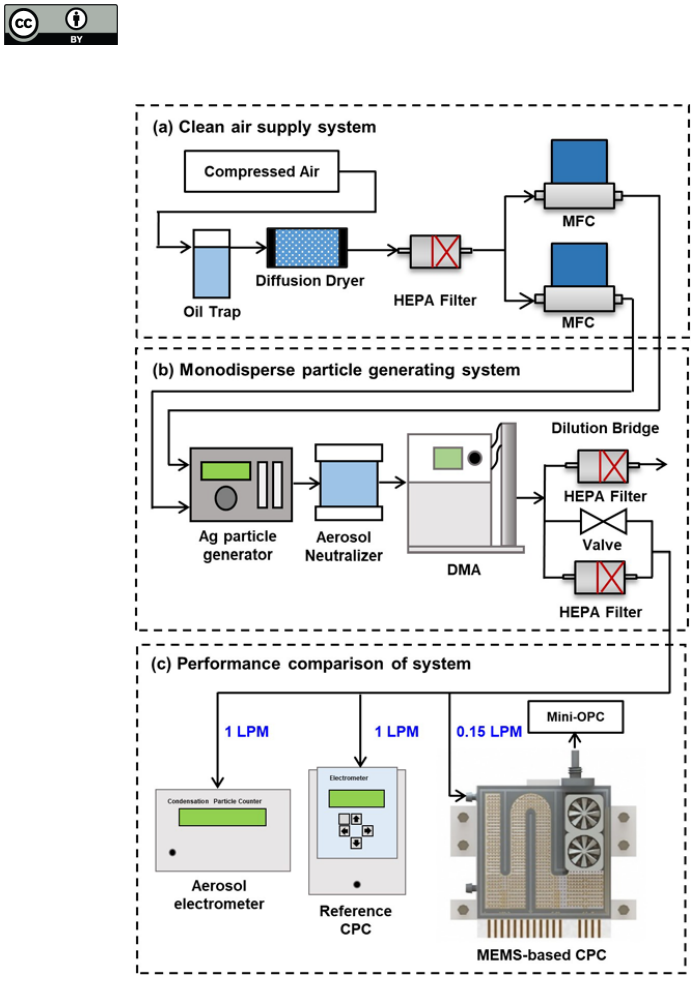

Figure 4: Schematic of the experimental setup for evaluating the performance of the MEMS-based CPC.

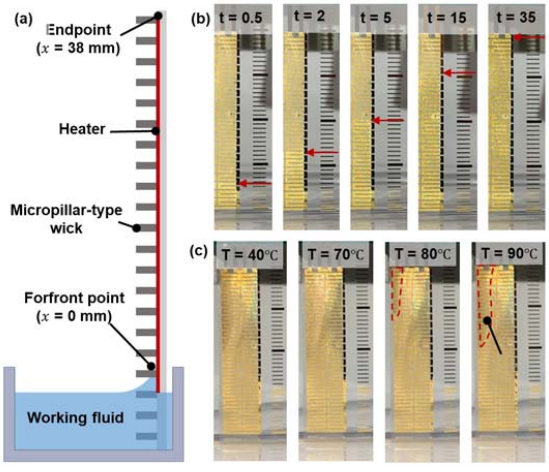

Figure 5: (a) Schematic of the capillary rise experimental setup; (b) selected video frames from the rise of the working fluid using micropillar-type wick; (c) the dry-out region formation as the surface temperature increased.

Atmos. Meas. Tech. Discuss., https://doi.org/10.5194/amt-2019-78
Manuscript under review for journal Atmos. Meas. Tech.
Discussion started: 6 March 2019

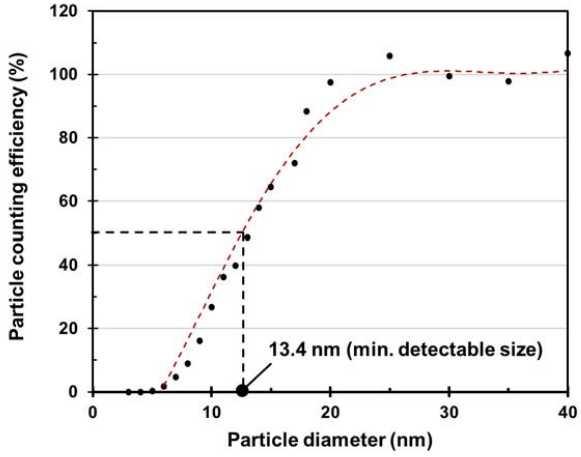

Figure 6: Particle counting efficiency of the MEMS-based CPC as a function of the particle size. The particle size at which the particle counting efficiency was fitted to 50% was 13.4 nm.

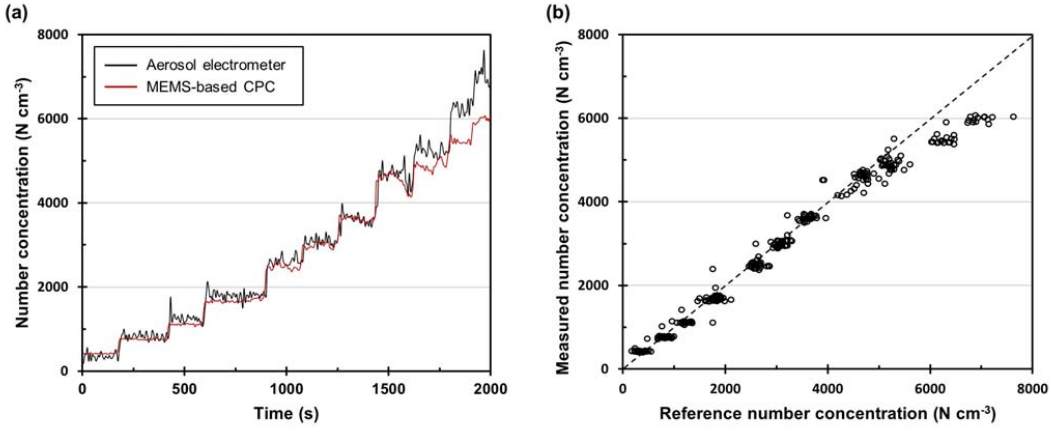

Figure 7: (a) Time series of the number concentrations with the MEMS-based CPC and aerosol electrometer; (b) one-to-one comparison of the measured number concentrations for both systems.

Atmos. Meas. Tech. Discuss., https://doi.org/10.5194/amt-2019-78
Manuscript under review for journal Atmos. Meas. Tech.
Discussion started: 6 March 2019

Atmospheric Measurement Techniques Discussions

Diameter (nm)		28	26	24	22	20	18	16
Number concentration ($N\ cm^{-3}$)	Reference CPC	8.36	18.99	223.84	585.87	1370.69	3733.96	4129.93
	MEMS-based CPC	7.99	17.65	224.58	619.10	1399.14	3809.45	4544.82
Difference (%)		4.55	7.60	-0.32	-5.37	-2.03	-1.98	-9.12

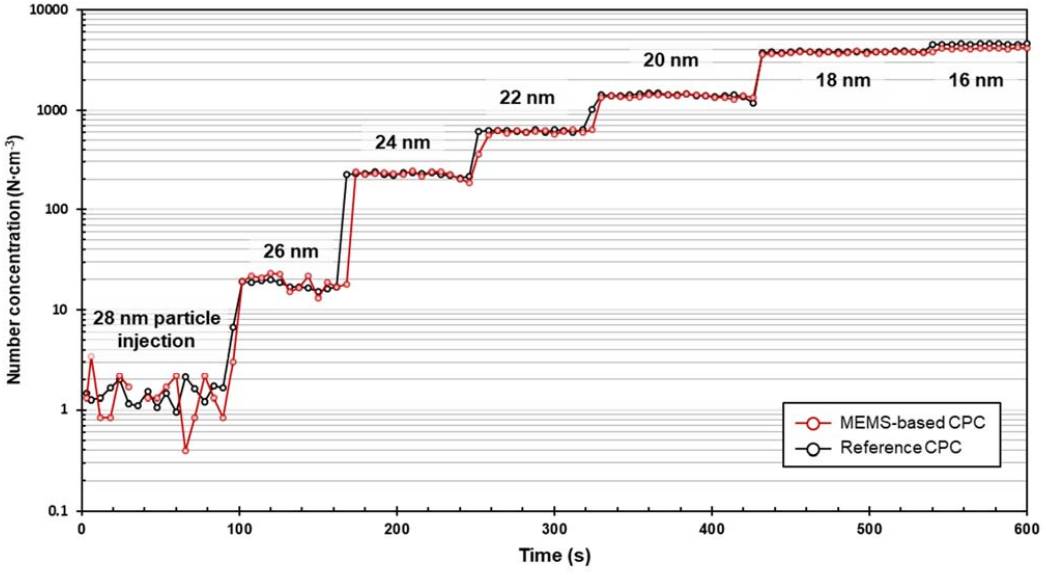

Figure 8: Time series of the number concentrations measured with the proposed system and reference CPC when the concentration and size were varied.